Nanoscale Res Lett (2010) 5:1948–1951
DOI 10.1007/s11671-010-9820-x

SPECIAL ISSUE ARTICLE

Deep-level Transient Spectroscopy of GaAs/AlGaAs Multi-Quantum Wells Grown on (100) and (311)B GaAs Substrates

M. Shafi · R. H. Mari · A. Khatab · D. Taylor · M. Henini

Received: 29 July 2010 / Accepted: 19 October 2010 / Published online: 16 November 2010
© The Author(s) 2010. This article is published with open access at Springerlink.com

Abstract Si-doped GaAs/AlGaAs multi-quantum wells structures grown by molecular beam epitaxy on (100) and (311)B GaAs substrates have been studied by using conventional deep-level transient spectroscopy (DLTS) and high-resolution Laplace DLTS techniques. One dominant electron-emitting level is observed in the quantum wells structure grown on (100) plane whose activation energy varies from 0.47 to 1.3 eV as junction electric field varies from zero field (edge of the depletion region) to 4.7×10^6 V/m. Two defect states with activation energies of 0.24 and 0.80 eV are detected in the structures grown on (311)B plane. The E_c-0.24 eV trap shows that its capture cross-section is strongly temperature dependent, whilst the other two traps show no such dependence. The value of the capture barrier energy of the trap at E_c-0.24 eV is 0.39 eV.

Keywords Laplace DLTS · Multi-quantum wells · DX centre · Heterostructures

Introduction

During last few decades, heterostructure-based devices have contributed to the advancement of diode lasers, high-speed electrical devices [1] and THz detectors [2]. Electrically and optically active defect states in the bandgap of semiconductor materials can play an important role in their carrier transport properties. Previous DLTS studies of defects in GaAs/AlAs/GaAs quantum wells [3] showed that at least six out of eight sub-bands in the heterostructures are occupied by defect states. Using DLTS technique, Jia et al. [4] investigated Si-doped GaAs/AlGaAs quantum wells and superlattices and demonstrated that the energy of the well-known DX centre in AlGaAs epilayers decreases in the case of multi-quantum wells and increases for superlattices. Arbaoui et al. [5] have also reported defects states in MBE-grown AlGaAs/GaAs multi-quantum well structures which can affect the carrier transport properties.

Most of the studies on defects in GaAs/AlGaAs quantum wells and superlattices reported so far are on samples grown on (100) GaAs plane. The crystallographic orientation of the substrate has a strong influence on incorporation of impurities and defects and hence on optical and electronic properties of III–V materials. It is therefore important to probe similar structures grown on non-(100) planes. In this work, DLTS [6] and LDLTS [7] techniques have been employed to investigate the electrical properties of defect states present within the bandgap of Si-doped GaAs/AlGaAs multi-quantum wells (MQWs).

Experimental Details

The n-type silicon-doped GaAs/AlGaAs MQWs were grown by molecular beam epitaxy (MBE) on a semi-insulating (100) and (311)B GaAs substrates. The epilayers that are doped to a concentration level of 2×10^{16} cm^{-3} are grown in the following order starting from the substrate: 1 μm GaAs buffer layer, 0.14 μm $Al_{0.33}Ga_{0.67}As$ barrier, a 60 periods GaAs (50Å)/$Al_{0.33}Ga_{0.67}As$ (90Å) MQWs, 0.14 μm $Al_{0.33}Ga_{0.67}As$ barrier. Ohmic contacts were made to the bottom n-type-doped GaAs buffer layer using wet chemical etching, metal evaporation of Ge/Au/Ni/Au (54-nm/60-nm/20-nm/136-nm-thick layers)

M. Shafi · R. H. Mari · A. Khatab · D. Taylor · M. Henini (✉)
School of Physics and Astronomy, Nottingham Nanotechnology & Nanoscience Centre, University of Nottingham, Nottingham NG7 2RD, UK
e-mail: mohamed.henini@nottingham.ac.uk

and annealing at 360°C for 30 s. The Schottky contacts were fabricated by evaporating Ti/Au (40 nm/175 nm) on the top of the n-type-doped $Al_{0.33}Ga_{0.67}As$.

Experimental Results

Current–voltage (I–V) measurements were taken prior to DLTS measurements to select the Schottky diodes with low leakage currents. Typical leakage currents of 2.4×10^{-9} and 1.2×10^{-9}A at reverse bias of −5 V were obtained on (100) and (311)B devices, respectively. Background doping concentration determined from capacitance–voltage (C–V) measurements was 1.64×10^{16} and 2.21×10^{16} cm^{-3} for (100) and (311)B samples, respectively. The devices were mounted in a 7-K closed-cycle helium cryostat. DLTS spectra obtained from both (100) and (311)B devices using a sampling rate window of 2.5 s^{-1}, a quiescent reverse bias of −5 V and a filling pulse of 1 ms are shown in Fig. 1a. LDLTS spectra of (100) and (311)B are shown in the inset of Fig. 1a. A prominent peak associated with the electron trap labelled E1 is detected in (100). The broader feature that appears in the tail of E1 at a temperature ~350 K could not be resolved by either technique. (311)B sample shows two peaks associated with defect states labelled EB1 and EB2. Trap EB1 appears as a shoulder of the main peak EB2 at temperature ~390 K and is resolved by using LDLTS as shown in the inset of Fig. 1a.

Carrier emission rates were determined at different temperatures using LDLTS. The value of the activation energy of each trap is determined by using the relation given by [6].

$$e_n = \sigma_n \langle V_{th} \rangle N_c \exp\left(-\frac{E_A}{k_B T}\right) \quad (1)$$

where E_A is the activation energy, σ_n is the capture cross-section, $<V_{th}>$ is the thermal velocity of the electron, N_c is the effective density of states in the conduction band, and k_B is the Boltzmann's constant.

The dependence of the emission rate signatures of trap E1 on the junction electric field is depicted in Fig. 2a as function of reverse bias. Electric field–dependent carrier emission measurements were taken using the double pulse method [8]. The activation energy of trap E1 determined from the slope of the Arrhenius plots (Fig. 2b) using Eq. 1 at different junction electric field strengths is illustrated in Fig. 2c. From the extrapolation of energy to the zero field value (edge of the depletion region) in the energy-field graph (Fig. 2c), the activation energy value varies from 0.47 to 1.3 eV as the electric field is varied from zero to 4.7×10^6 V/m.

The emission rates of traps EB1 and EB2 in (311)B samples show no dependence on the junction electric field,

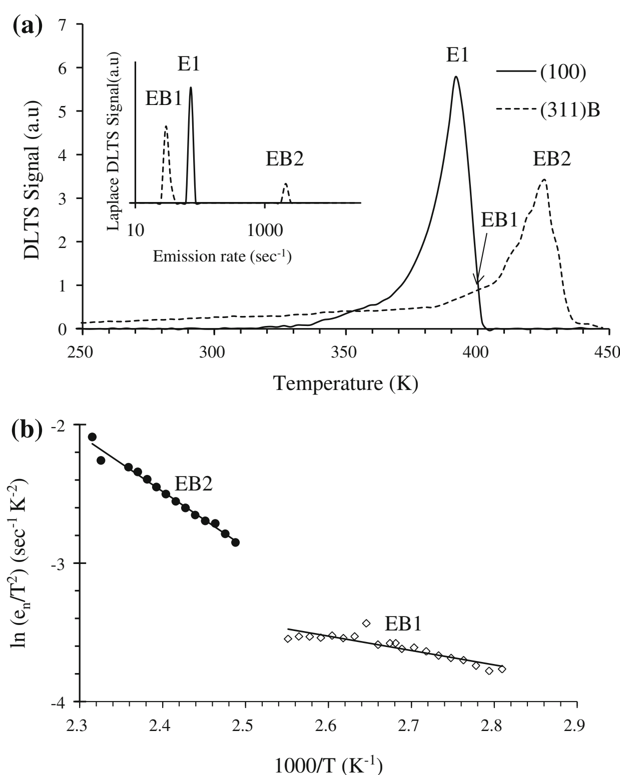

Fig. 1 **a** DLTS spectra of GaAs/AlGaAs multi-quantum well structures grown on (100) and (311)B GaAs substrates. The inset shows the peaks resolved by Laplace DLTS technique; **b** Activation energies of defect states EB1 and EB2 in (311)B samples as determined from the Arrhenius plots

and their activation energies as determined from Arrhenius plots (Fig. 1b) are 0.24 and 0.80 eV, respectively.

Direct carrier capture measurements have also been carried out using filling pulse method [9] at different temperatures using the relation given below

$$\Delta C(t_p) = \Delta C_{max}\left[1 - \exp\left(\frac{-t_p}{\tau_c}\right)\right] \quad (2)$$

where ΔC is the magnitude of the capacitance transient, t_p is the applied pulse duration, and τ_c is the capture coefficient. The value of τ_c is derived from Eq. 2 and σ_n is determined using the following relation [9].

$$\sigma_n = \frac{1}{\tau_c \langle V_{th} \rangle n} \quad (3)$$

where n is the free carrier concentration.

The inset of Fig. 3a, b, c shows σ_n as function of temperature for traps in (100) and (311)B samples. σ_n of trap EB1 (Fig. 3c, and the inset) shows a strong dependence on the temperature, whilst σ_n of E1 and EB2 (Fig. 3a, b and the insets) are temperature independent. The capture barrier energy is determined using the relation given below [10].

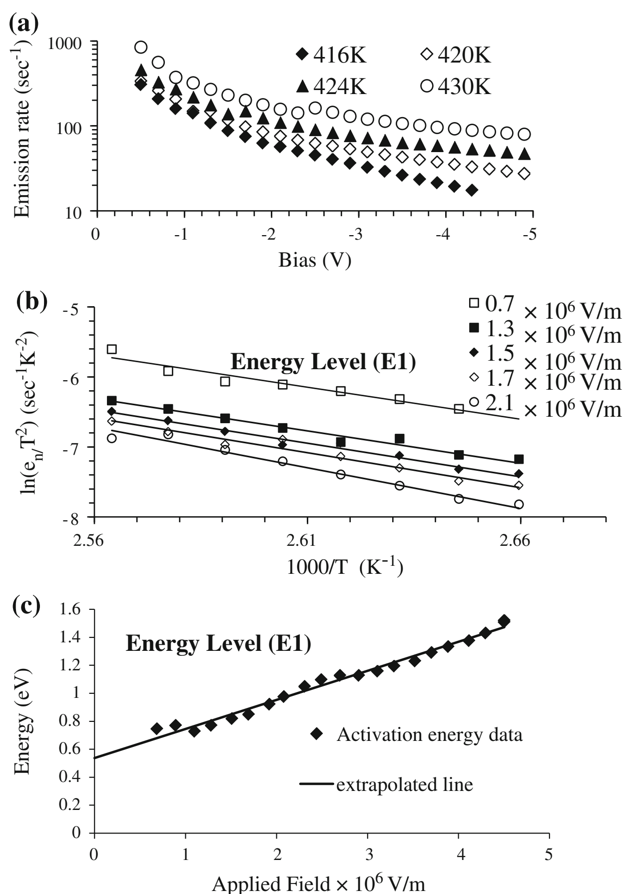

Fig. 2 Emission rate signatures of each defect state; **a** Illustration of the bias dependence of the emission rates of E1; **b** Arrhenius plots obtained from the thermal emission rates at different junction fields; **c** Activation energy of trap E1 as a function of applied electric field

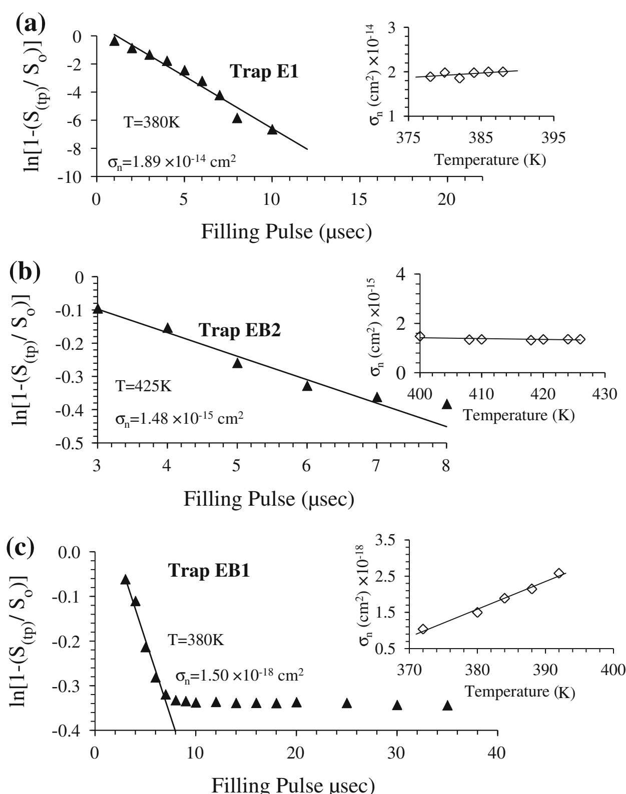

Fig. 3 Capture cross-section measurement for **a** trap E1, **b** trap EB2 and **c** trap EB1. Temperature effect on capture cross-section for each trap is shown in the insets

$$\sigma_n(T) = \sigma_\infty \exp\left(\frac{-E_\infty}{k_B T}\right) \quad (4)$$

where E_∞ is the energy barrier to capturing electrons and σ_∞ is the apparent value of the capture cross-section.

Discussion

Our results demonstrate that trap E1 in (100) sample is strongly influenced by the external applied electric field. The broad feature that appears in the tail of this peak could be due to the existence of a closely spaced defect that cannot be resolved because of its very small concentration. We observed that the emission rates in the 416–430 K temperature range of trap E1 (Fig. 2a) decrease as the junction reverse bias increases. This kind of behaviour is not compatible within the framework of the well-known Poole–Frenkel mechanism in which the emission rate is enhanced with the increase in the junction electric field [11]. However, this sort of trend of carrier emission as a function of electric field has also been observed for DX-related centres in GaAs/AlGaAs MQWs structures by Jia et al. [12]. In addition, this effect was found to be dependent on the Al composition. Their results show that the decrease in the thermal emission rates with increasing field is strongest for the layers having medium Al compositions (Al: 30–40%) and smallest for the large Al content layers (Al: 50–60%). Our emission rates versus electrical field results in the MQWs samples which have a 33% Al composition confirm their observations.

Further, the emission rates decrease with increasing field strengths, which is contrary to the Poole–Frenkel effect. Jia et al. [12] suggested that these changes in the emission and capture rates at different field strengths are due to the traps which are closely located and interacting with each other. Moreover, if the electric field is not uniform in the depletion region of the Schottky junction, emission rates contribute non-uniformly from the depletion layer edge (zero field) to the maximum junction field [13]. This infers that the decrease in the carrier emission rate of E1 might be due to its interaction with some other traps such as the one that appears in the tail of its DLTS signal.

The dependence of the emission rate on the electric field indicates that the trap can acquire a different net charge

after the emission of the carriers from the trap. The trap E1 is electrically charged upon electron emission, and it becomes neutral by capturing an electron. This suggests that E1 should be a donor-like level. From the activation energy results (Fig. 2c) for E1, the exact location of the trap in the bandgap of the material is difficult to identify. At zero field, extrapolation for the activation energy in Fig. 2c gives the value of 0.47 eV which could correspond to DX centre.

Since Laplace DLTS was able to resolve the broad peak in (311)B sample, thermal emission rates of both traps (EB1 and EB2) were analysed separately at different reverse biases and no such behaviour to what we have seen in the (100) sample has been observed. Thus, the emission rate signatures of EB1 and EB2 are electric field independent, and their charge state is neutral. The activation energies determined from their emission rates using Eq. 1 are 0.24 and 0.80 eV, respectively. The emission rate signatures of EB2 are comparable with published data of defect E4 studied by Hayakaw et al. [13] in MBE-grown Si-doped AlGaAs layers. They have considered the influence of stoichiometry on the traps and assigned this trap to a complex that can include both group III vacancy (arsenic-interstitial or antisite defect As_{III}) and the arsenic vacancy (group III interstitial or III_{As}).

The capture cross-section (σ_n) results determined at different temperatures show that carrier capture rates are thermally activated for EB1(inset of Fig. 3c), whereas the defect states E1 and EB2 show no such dependence upon temperature as depicted in insets of Fig. 3a, b. Although σ_n of E1 does not depend on the temperature, but due to the strong influence of the junction field, the apparent capture cross-section determined from the intercept of the Arrhenius plot of the emission rates shows large fluctuations in its value from 1.75×10^{-15} to 3.45×10^{-10} cm^2 as the field varies from zero to 4.7×10^6 V/m. The direct capture cross-section measurements of this trap (Fig. 3a) at 380 K and applied bias of -5 V give a value of 1.89×10^{-14} cm^2, which is much smaller than its apparent value. The value of capture cross-section of trap EB2 (Fig. 3b) is found to be 1.48×10^{-15} cm^2. The inset of Fig. 3c clearly shows the increase of σ_n from 1.04×10^{-18} to 2.58×10^{-18} cm^2 as the temperature increases from 372 to 392 K. The capture barrier energy calculated using relation (4) is 0.39 eV, which suggests a strong interaction of carriers with the lattice [14].

Conclusion

We reported here the DLTS and LDLTS studies of MQWs samples grown by MBE on (100) and (311)B GaAs substrates. The activation energy of the dominant trap E1 observed in the sample grown on (100) is found to be dependent on the junction electrical field. The measured value for this trap varies from 0.47 to 1.3 eV as junction electric field varies from zero to 4.7×10^6 V/m. Since the emission rates of E1 are dependent on electric field, it can be concluded that E1 is a donor-like level. Since EB1 and EB2 traps in (311)B showed no evidence of a field dependence, their charge states are confirmed to be neutral. In addition, we observed that the capture cross-section of EB1 is thermally activated, while those of E1 and EB2 are not.

Open Access This article is distributed under the terms of the Creative Commons Attribution Noncommercial License which permits any noncommercial use, distribution, and reproduction in any medium, provided the original author(s) and source are credited.

References

1. R. Ajjel, H. Maaref, Microelectronics. J. **37**, 1404 (2006)
2. M. Kagan, I. Altukhov, E. Chirkova, V. Sinis, R. Troeger, S. Ray, J. Kolodzey, Physica. Status. Solidi. (b) **235**, 135 (2003)
3. Q. Zhu, Z. Gu, Z. Zhong, Z. Zhou, L. Lu, Appl. Phys. Lett. **67**, 3593 (1995)
4. Y. Jia, Z. Han, H. Grimmeiss, L. Dobaczewski, J. Appl. Phys. **80**, 2860 (1996)
5. A. Arbaoui, B. Tuck, C.J. Paull, M. Henini, J. Mat. Sci. **1**, 75 (1990)
6. D.V. Lang, J. Appl. Phys. **45**, 3023 (1974)
7. L. Dobaczewski, A. Peaker, K. Nielsen, J. Appl. Phys. **96**, 4689 (2004)
8. V.P. Markevich, A.R. Peaker, V.V. Litvinov, L.I. Murin, N.V. Abrosimov, Physica. B. **376**, 200 (2006)
9. Akbar Ali, M. Shafi, Abdul Majid, Phys. Scr. **74**, 450 (2006)
10. C.H. Henry, D.V. Lang, Phys. Rev. B. **15**, 989 (1977)
11. J. Frenkel, Phys. Rev. **54**, 647 (1938)
12. Y.B. Jia, H.G. Grimmeiss, Phys. Rev. B. **47**, 1858 (1993)
13. C.Y. Chang, W.C. Hsu, S.J. Wang, S.S. Hau, J. Appl. Phys. **60**, 1042 (1986)
14. T. Hayakawa, M. Kondo, T. Suyama, K. Takahashi, S. Yamamoto, S. Yano, T. Hijikata, Appl. Phys. Lett. **49**, 788 (1986)